Molecular Imaging
Volume 19: 1-9

DOI: 10.1177/1536012120968669
journals.sagepub.com/home/mix
SAGE

[^{11}C]Methionine and [^{11}C]PBR28 as PET Imaging Tracers to Differentiate Metastatic Tumor Recurrence or Radiation Necrosis

Thuy T. Tran, MD, PhD[1], Jean-Dominique Gallezot, PhD[2], Lucia B. Jilaveanu, MD, PhD[1], Christopher Zito, PhD[3], Gabriela Turcu, MD[1], Keunpoong Lim, PhD[2], Nabeel Nabulsi, PhD[2], Henry Huang, PhD[2], Anita Huttner, MD[4], Harriet M. Kluger, MD[1], Veronica L. Chiang, MD[1,5], and Richard Carson, PhD[2]

Abstract

Purpose: As stereotactic radiosurgery (SRS) and immunotherapy are increasingly used to treat brain metastases, incidence of radiation necrosis (RN) is consequently rising. Differentiating tumor regrowth (TR) from RN is vital in management but difficult to assess using MRI. We hypothesized that tumor methionine levels would be elevated given increased metabolism and high amino acid uptake, whereas RN would increase inflammation marked by upregulated translocator protein (PBR-TSPO), which can be quantified with specific PET tracers.

Procedures: We performed a feasibility study to prospectively evaluate [^{11}C]methionine and [^{11}C]PBR28 using PET in 5 patients with 7 previously SRS-treated brain metastases demonstrating regrowth to differentiate TR from RN.

Results: Sequential imaging with dual tracers was well-tolerated. [^{11}C]methionine was accurate for detecting pathologically confirmed TR in 7/7 lesions, whereas [^{11}C]PBR28 was only accurate in 3/7 lesions. Tumor PBR-TSPO expression was elevated in both melanoma and lung cancer cells, contributing to lack of specificity of [^{11}C]PBR28-PET.

Conclusion: Sequential use of PET tracers is safe and effective. [^{11}C]Methionine was a reliable TR marker, but [^{11}C]PBR28 was not a reliable marker of RN. Studies are needed to determine the causes of post-radiation inflammation and identify specific markers of RN to improve diagnostic imaging.

Keywords

brain metastasis, PET, radiation necrosis, [^{11}C]methionine, [^{11}C]PBR28

Introduction

The understanding and treatment of metastatic brain tumors remains a significant clinical challenge owing to the difficulty of obtaining tissue, variable blood-brain barrier drug penetration, and limited drug intracranial efficacy. The morbidity of surgery makes less invasive options such as radiation and systemic therapy attractive. Stereotactic radiosurgery (SRS) provides precision tumor ablation while largely sparing surrounding brain via focused, high-dose radiation, thus producing superior local control with less cognitive dysfunction compared to whole-brain radiation. SRS has thus gained popularity as first-line treatment of brain metastases (BMs) and as salvage when whole-brain radiation fails.

[1] Yale School of Medicine and Yale Cancer Center, Yale University, New Haven, CT, USA
[2] Department of Radiology and Biomedical Imaging, Yale School of Medicine, Yale University, New Haven, CT, USA
[3] Department of Biology, School of Health and Natural Sciences, University of Saint Joseph, West Hartford, CT, USA
[4] Department of Pathology, Yale School of Medicine, Yale University, New Haven, CT, USA
[5] Department of Neurosurgery, Yale School of Medicine, Yale University, New Haven, CT, USA

Submitted: 19/05/2020. Revised: 31/08/2020. Accepted: 17/09/2020.

Corresponding Author:
Thuy T. Tran, Yale Cancer Center, 333 Cedar Street, PO Box 208028, New Haven, CT 06520, USA.
Email: thuy.tran@yale.edu

Adding immunotherapy to SRS has further improved intracranial disease control but increases radiation necrosis (RN) up to 68%.[1] RN is histologically defined by coagulative necrosis surrounded by post-radiation changes, including macrophage infiltration, demyelination, vascular hyalinization, and reactive astrocytosis. Differentiating tumor recurrence (TR) from RN is easy histologically but difficult radiographically. Since no current single imaging parameter reliably differentiates RN from TR, surgical biopsy remains the diagnostic gold standard.[2]

Newer imaging radiotracers for positron emission tomography (PET) are being developed to exploit the divergent pathophysiology of TR and RN and circumvent tissue sampling needs. Primary brain tumors are noted to overexpress amino acid transporters and increase amino acid uptake compared to normal brain.[3] The most promising amino acid imaging tracers include ^{18}Fluoro-O-(2) fluoroethyl-l-tyrosine ([^{18}F]FET),[4-6] [^{11}C] Methionine (MET), and ^{18}F-dihydroxyphenylalanine (^{18}F-DOPA) are similarly sensitive and specific for tumor regrowth.[7] Studies primarily in gliomas have reported [^{11}C]MET has 70-100% sensitivity and 60-100% specificity for TR.[8-12] The wide sensitivity and specificity ranges for [^{11}C]MET are based on different standard uptake value (SUV) cutoffs, and new guidelines have recently been published to help standardize imaging in gliomas.[13]

Levels of translocator protein (TSPO), also known as peripheral benzodiazepine receptor (PBR), increase in pathological states associated with microglial activation. PBR-TSPO has been successfully used in human studies assessing neuroinflammation in multiple sclerosis, amyotrophic lateral sclerosis, and Alzheimer's disease.[14] Tumors of adrenals, testis, liver, and skin, including melanoma,[15] showed lower PBR-TSPO expression compared with normal tissue, although little is known about PBR-TSPO expression in BMs.[16] Although PBR-TSPO expression has not been directly evaluated in RN, the neuroinflammatory process, characterized by microglial activation and reactive gliosis, known to upregulate expression is well-established.[17-19] PBR-TSPO expression could therefore be a potential adjunctive marker to complement [^{11}C]MET in differentiating TR from RN. Previous generations of PBR-TSPO targeting PET tracers have been tested, such as [^{11}C]PK11195 but are currently replaced by newer, more selective agents, such as [^{11}C]PBR28.

We hypothesized that in RN, MRI enhancement is related to inflammation and microglial activation[20]; [^{11}C]PBR28, a second-generation PET tracer that binds to PBR-TSPO, can be used in conjunction with [^{11}C]MET to improve the diagnostic ability of PET in differentiating RN and TR.[21] We performed a small, prospective study evaluating the feasibility of sequential [^{11}C]MET and [^{11}C]PBR28 PET tracers in patients with previously SRS-treated BMs who have enlarging lesions on follow-up imaging, NCT02433171. The study anticipated accruing 20 melanoma and 20 lung cancer patients but was terminated early after enrolling 5 patients due to the failure of [^{11}C]PBR28 imaging for this application. Here, we present data on the 5 patients evaluated.

Materials and Methods

Patients

NCT02433171 was a prospective pilot study performed at the Yale Cancer Center and Yale School of Medicine in patients with progressively enhancing metastatic brain lesions previously treated with SRS. Patients were recruited from January to August 2015 with last follow-up scan completed 1 year after enrollment. Primary outcome measure was whether TR versus RN determined by PET imaging was confirmed by pathology or serial imaging. Eligibility criteria included age 18-80 years, regrowing melanoma or non-small cell lung cancer BMs following prior SRS, candidates for surgical intervention, or asymptomatic with a >6-month life expectancy amenable to monitoring by serial imaging. Exclusion criteria included exceeding United States Food and Drug Administration annual radiation limits within the year prior to enrollment (>5 REM per year), pregnant or breastfeeding, sexually active women of child-bearing age unless on 2 forms of contraception with negative pregnancy testing, or inability to undergo gadolinium-based MRI. All eligible lesions received gamma knife only since detection; patients were identified by MRI enhancement of previously treated lesions. Each intracranial lesion was evaluated as a unit of analysis. After imaging, intracranial lesions were biopsied or resected, or subjects continued to undergo serial MRI over 6 months. Stable or spontaneously resolving lesions on imaging were assumed to represent RN. A total of 5 patients were enrolled, and all patients underwent imaging with a total of 7 intracranial lesions. All lesions were evaluable.

[^{11}C]MET and [^{11}C]PBR28 PET Imaging

Dosing and tolerability were previously established separately for the PET tracers [^{11}C]MET and [^{11}C]PBR28.[22,23] Imaging was performed using a high-resolution research tomograph (HRRT) PET scanner and combined with event-by-event head motion correction,[24] using MOLAR (Motion-compensation OSEM List-mode Algorithm for Resolution-recovery reconstruction) and the Vicra system (NDI, Waterloo, Canada).[25] For [^{11}C]MET studies, 517 $\pm$ 203 MBq of radiotracer was intravenously injected, and a 60-min dynamic scan was acquired. For [^{11}C]PBR28 studies, 670 $\pm$ 89 MBq of radiotracer was injected, and a 120-min dynamic scan was acquired. Frame duration was 6 $\times$ 30 sec, 3 $\times$ 1 min, 2 $\times$ 2 min, then 10 $\times$ 5 min for [^{11}C]MET and 22 $\times$ 5 min for [^{11}C]PBR28 scans. Arterial sampling was performed in 4/5 subjects to measure the input function used in kinetic modeling of PET data. The fifth patient was on long-term anticoagulation and could not safely undergo arterial sampling. Blood was assayed using a cross-calibrated gamma counter and by HPLC to measure the fraction of unmetabolized parent radiotracer.

Summed images (0–10 min post-injection) were created from the motion-corrected PET and registered to the subject's MPRAGE image. Three regions of interest (ROIs) were defined on MRI and co-registered to the PET for tumor and normal brain: ROI over the lesion's gadolinium enhancement, over normal/contralateral cortical tissue, and over normal cerebellum. ROI time-activity curves were generated, and kinetic analysis was applied. For [^{11}C]MET, the uptake rate constant K_i was estimated using Patlak analysis[26,27] when the blood input functions were available. For [^{11}C]PBR28, the volume of distribution V_T was estimated using multilinear analysis-1 (MA1)[28] when the blood input functions were available, and the distribution volume ratio (*DVR*) was estimated using the multilinear reference tissue method (MRTM),[29] with normal, contralateral cortical tissue as a reference region. In addition to regional kinetic parameters, parametric images of the kinetic parameters were obtained. SUV values were computed at 20-60 min post-injection for [^{11}C]MET and 40-60 min post-injection for [^{11}C]PBR28. In all cases, tumor-to-normal (benign/contralateral tissue) brain ratios of kinetic parameters (K_i ratio or distribution volume ratio: *DVR*) and SUV (SUVR: SUV ratio) were determined. Given the nature of the study, image analysis results were not blinded to the final diagnosis of TR or RN.

PBR-TSPO Protein Analysis in Human Cell Lysates

Total protein was collected from 3 human monocyte (gift from Dr. Madhav Dhodapkar, Yale), 3 human lung (ATCC), and 6 human melanoma cultures (derived at Yale University). Primary cell cultures derived at Yale were used within 20 passages and routinely tested to exclude mycoplasma. Immunoblotting using anti-rabbit anti-PBR (Abcam, ab109497, 1:10,000) and β-actin (Sigma, A5441, 1:500) was conducted by standard methods, and band intensity was quantified relative to β-actin using Image J (NIH).

PBR-TSPO Staining of Human NSCLC and Melanoma Tissue

Tissue microarrays containing formalin-fixed, paraffin-embedded tumor from patients with NSCLC or melanoma were stained using the EnVision system (Dako, 4003 and 4001) with rabbit anti-PBR (Abcam, ab109497, 1:20,000) on Cy-5 (Perkin Elmer, SAT705A001) and either mouse pan-cytokeratin (DAKO, M3515, 1:50) for NSCLC or S100 (BioGenex, MU058-UC, 1:50) for melanoma on Cy-3 (Perkin Elmer, SAT704A001), and DAPI (Thermo Fisher Scientific, 62248, 1:50). Automated quantitative image analysis was done as detailed previously.[30] PBR-TSPO signal was normalized to the tumor mask area, defined by either the cytokeratin or S100 signal, and then scored on a scale of 0 to 255.

Statistics

For tracer signal assessment in ROIs, the main kinetic parameter of interest for [^{11}C]MET was the uptake rate constant K_i; SUV, SUVR and K_i ratio, relative to the contralateral ROI, were also assessed. For [^{11}C]PBR28, due to the high inter-subject variability of V_T values, in part due to a genetic polymorphism affecting [^{11}C]PBR28 binding,[31] the main kinetic parameter of interest was the V_T ratio (*DVR*). Inter-subject variability due to this polymorphism is minimized by using the ratio of affected to contralateral unaffected brain for each individual patient. [^{11}C]PBR28 SUV and SUVR were not used due to the poor correlation between V_T and SUV(R) values for this tracer. To determine if the value of a kinetic parameter ([^{11}C]MET K_i, K_i ratio, SUV, SUVR or [^{11}C]PBR28 *DVR*) was elevated in the main ROI, the mean and standard deviation for each parameter was determined in the cerebellum, and a threshold was selected as the mean plus 6 standard deviations, based on visual assessment. Unpaired t-tests were used to compare average band intensity for NSCLC and melanoma cells with monocyte cell lines and for immunofluorescence analysis (GraphPad Prism).

Study Approval

Approval for this study was obtained from the Yale Institutional Review Board and done in accordance with the 1964 Helsinki declaration and its later amendments. All subjects signed informed consent prior to enrollment.

Results

Serial [^{11}C]MET and [^{11}C]PBR28 PET Imaging Was Feasible and Well-Tolerated

Five patients (3 melanoma and 2 NSCLC patients, 3 males, ages 55-82) with 7 SRS-treated BMs (size range 1.83-2.90 cm) were enrolled and imaged without complications. All lesions were located in the cerebrum and were prescribed SRS (18-22 Gy) (Table 1). Time from SRS to PET imaging ranged from 8 to 21 months. Histology was obtained in 4 out of the 7 lesions imaged: 2 demonstrated TR, and 2 showed RN. The remaining 3 lesions were deemed RN due to radiographic stability for a minimum of 8.5 months. Given the short half-life of C-11 radioisotope, it was feasible to complete dual tracer imaging sequentially for all patients (total time $\sim$5 h).

[^{11}C]MET Is a Reliable Tracer for Detecting Local Recurrence in Brain Metastatic Disease

[^{11}C]MET SUV or SUVR values were well correlated with [^{11}C]MET K_i values ($r^2 = 0.981$ for SUV, $r^2 = 0.935$ for SUVR), indicating that SUV or SUVR (reference: normal contralateral tissue) is suitable for alternate simplified quantification of [^{11}C]MET uptake (Supplemental Figure S1). Consequently, SUV(R) images and K_i images were visually similar. Using a combination of visual inspection and quantitative analysis, [^{11}C]MET was accurate in differentiating TR and RN in 7/7 lesions. All [^{11}C]MET positive lesions were pathologically confirmed to have TR, and all negative lesions

Table 1. Patient Demographics and Results of [^{11}C]MET and [^{11}C]PBR28 PET in SRS-Treated Patients.

Patient ID	Diagnosis	Tumor location	Sex	Age	Mutations	Months since SRS	Radiation dose (Gy)	Systemic therapy	Concurrent steroids	[^{11}C]MET	[^{11}C]PBR28	Pathology	Imaging follow-up (Months)
1	Melanoma	Right frontal	M	82	BRAF mutant	13.4	20	ArQule-736 (pan-RAF inhibitor); nivolumab	None	+	+	Tumor with RN	
2	NSCLC	Right frontal	F	55	None	21.3	22	Cisplatin/etoposide	None	+	+	Tumor	
3	Melanoma	Right frontal	M	56	BRAF wild-type	20.1	20	High dose IL-2; ipilimumab; pembrolizumab	None	−	−	RN	
4	NSCLC	Left frontal	F	63	None	11.9	18	Carboplatin/pemetrexed	Yes	−	−	Presumed RN	8.5
		Right parietal				11.9	18			−	−	Presumed RN	8.5
5	NSCLC	Right frontal	M	62	KRAS mutant	8.3	18*	Carboplatin/paclitaxel	Yes	−	+	Presumed RN	12.5
		Left frontal				8.3	18*			−	+	RN	

*Patient also had prior WBRT.

did not have viable tumor on pathology or were deemed RN via stable longitudinal imaging (Table 1 and Supplemental Table S1). Representative radiographic images and pathology are depicted in Figure 1.

[^{11}C]PBR28 Is Not a Reliable Tracer for Detecting Radiation Necrosis in Brain Metastatic Disease

[^{11}C]PBR28 SUV or SUVR values were poorly correlated with [^{11}C]PBR28 V_T values ($r^2 = 0.483$ for SUV, $r^2 = 0.039$ for SUVR versus V_T, $r^2 = 0.23$ for SUVR vs *DVR*), indicating that SUV or SUVR is not suitable for simplified quantification of [^{11}C]PBR28 binding in BMs. Since arterial input function data were not available for 1 subject, and SUV or SUVR was not suitable for [^{11}C]PBR28, MRTM was applied to all [^{11}C]PBR28 studies. *DVR* values obtained with MA1 and MRTM were compared for the first 4 subjects. MA1 and MRTM values were highly correlated ($r^2 = 0.870$, Supplemental Figure S2), indicating that MRTM could be used to quantify [^{11}C]PBR28 *DVR* values (Table 1 and Supplemental Table S2).

[^{11}C]PBR28 only had a diagnostic accuracy of identifying RN in 3/7 lesions. Of the 5 patients with 7 BMs imaged, 4 lesions were positive for [^{11}C]PBR28 using a threshold of *DVR* >1.77. Patients 1 and 5 had lesions with RN and demonstrated corresponding [^{11}C]PBR28 avidity. However, patient 2 had false positivity, and patients 3 and 4 had false negativity to [^{11}C]PBR28 uptake (Table 1). Interestingly, patient 1 had a mix of tumor and RN, and PET imaging confirmed dual positivity for [^{11}C]MET and [^{11}C]PBR28. Given the poor accuracy of [^{11}C]PBR28 in identifying RN, this tracer would not be reliable for clinical use.

PBR-TSPO is associated with inflammation, and we attempted to determine whether the poor accuracy of [^{11}C]PBR28 was due to confounders such as concurrent corticosteroid or checkpoint inhibitor use. [^{11}C]PBR28 was detectable in 50% of lesions treated with corticosteroids. Moreover, receipt of concurrent anti-PD1 did not increase [^{11}C]PBR28 avidity; ultimately, patient 3 had a false negative result, as biopsy confirmed RN (Table 1). Although our sample size was small, these confounders were not clear contributors to the low accuracy of [^{11}C]PBR28 in detecting RN, prompting us to search for other factors.

Limited Utility of [^{11}C]PBR28 Due to PBR-TSPO Expression in NSCLC and Melanoma

To determine what factors contributed to the false positive cases in [^{11}C]PBR28 uptake, we performed an exploratory analysis evaluating PBR-TSPO expression in NSCLC and melanoma cells using a combination of human cell lines and biopsy tissue. We found that NSCLC and melanoma cells express 62% and 60% less PBR-TSPO, respectively, compared to monocyte cells (Figure 2A-B). Although expression is decreased, levels of PBR-TSPO detected on human tissue microarrays was clearly measurable (Figure 2C-D).

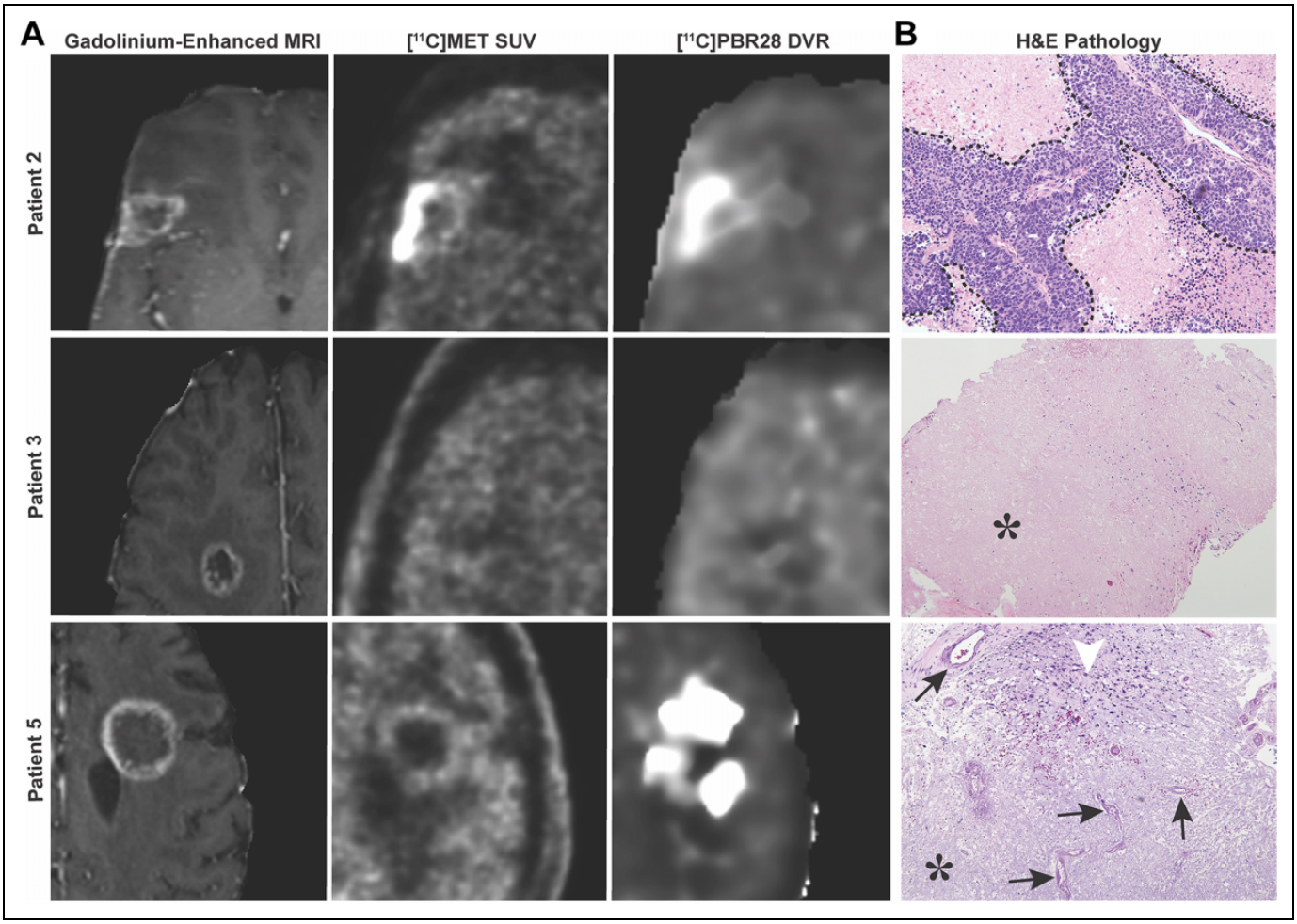

Figure 1. MRI and PET imaging for [11C]MET and [11C]PBR28. A, Representative images of suspicious lesions for TR or RN as seen on post-gadolinium MRI sequences. Corresponding lesions as seen on PET for [11C]MET and [11C]PBR28. B, Patient 2 had histologically confirmed TR, but had uptake of both [11C]MET and [11C]PBR28 radiotracers. Patient 3 had histologically confirmed RN but had absent uptake of both [11C]MET and [11C]PBR28 radiotracers. Patient 5 had histologically confirmed RN and demonstrated uptake of only [11C]PBR28. Tumor is outlined in a dashed line (top photo, taken at 20X). Characteristic features of RN include vessel hyalinization (arrows), increased immune infiltrate (arrowhead) (bottom photo, taken at 10X), and paucicelluar coagulative necrosis (*) (middle photo, taken at 4X, and bottom photo).

Discussion

Our goal was to identify PET radiotracers that can differentiate RN from TR. While the gold standard remains histopathologic evaluation, surgical intervention for tissue is a morbid procedure, requires short-term steroids perioperatively, necessitates adequate wound healing before subsequent therapy, and can be contraindicated with recent anti-vascular endothelial growth factor therapy. PET imaging studies using single tracers have been previously employed to help differentiate TR from RN with varying degrees of success. The most promising agents to date have been [^{11}C]MET, [^{18}F]FET, and [^{18}F]DOPA, but implementation into standard practice has been limited to larger academic centers due to tracer stability.[9] Our goal was to determine whether adding a sequential PET tracer to [^{11}C]MET to image inflammation was feasible and would improve the ability to differentiate TR and RN. This is the first report assessing [^{11}C]PBR28 for its ability to distinguish TR and RN. The only other clinical trial using [^{11}C]PBR28, NCT02431572, completed recruitment and evaluated patients with glioblastoma or melanoma BMs, but final results are not yet published. This is also the first study evaluating sequential, dual tracer PET scans to improve upon existing imaging techniques in differentiating TR and RN. Most studies using these PET imaging tracers have focused on primary brain malignancies; our study contributes data on the use of these tracers in metastatic brain cancer. Furthermore, our study employed an HRRT scanner, the highest resolution human brain scanner available. This new technology was utilized to improve the diagnostic resolution and provided another innovation in our approach.

Although a small study, the 5 patients enrolled had representative demographics for melanoma and NSCLC patients with BMs. None of the patients enrolled had complications arising from dual PET tracer imaging procedures. For

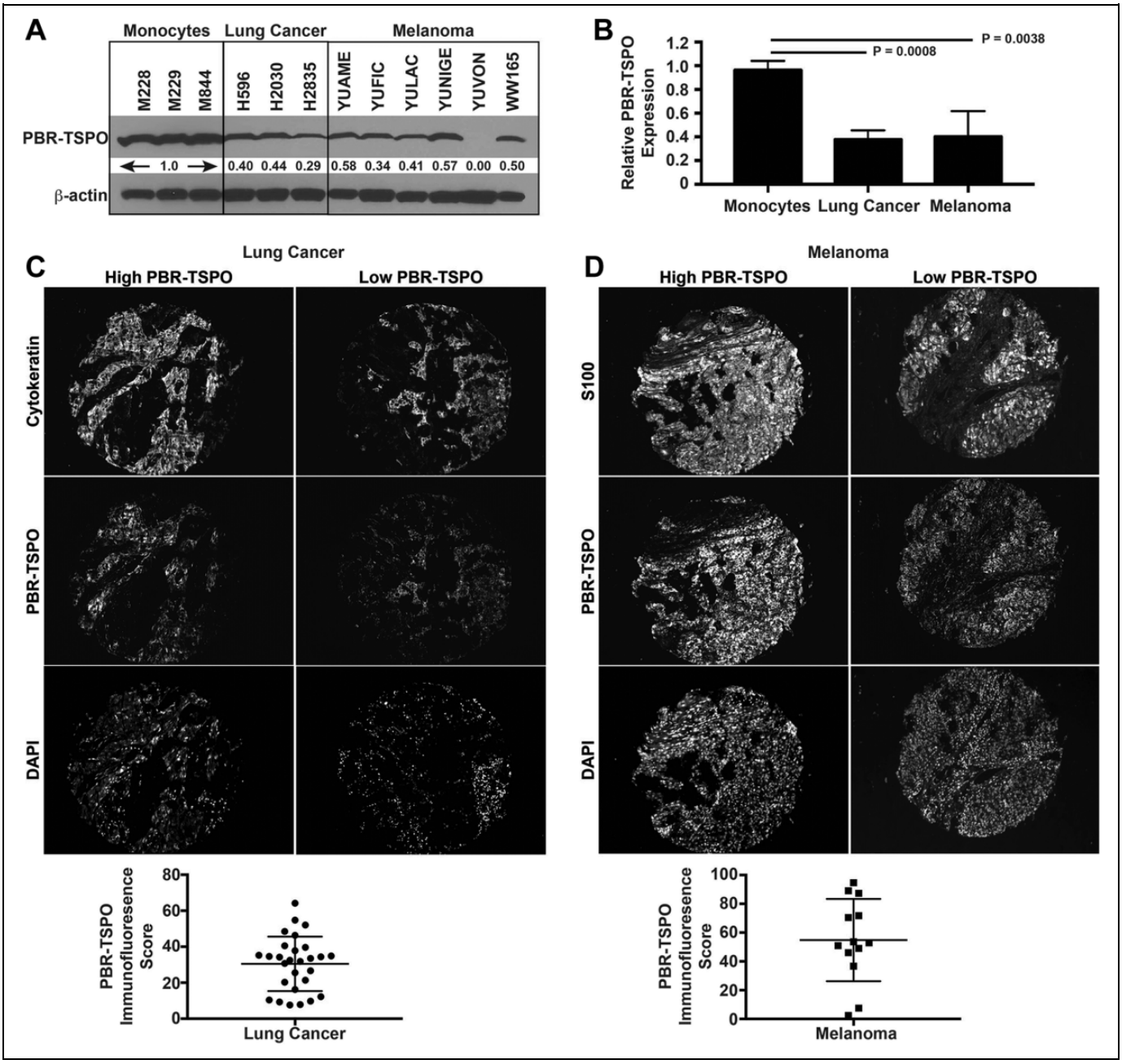

Figure 2. Quantitation of PBR-TSPO in NSCLC and melanoma. (A-B) PBR, also known as TSPO, protein is present at high levels in human monocytes, but expression is decreased in human NSCLC ($P = 0.0038$ by t test, mean 0.38 ± 0.045 standard error of the mean [SEM]) and human melanoma ($P = 0.0008$, 0.40 ± 0.089) cell lines. (C) Human NSCLC ($n = 28$) and (D) melanoma ($n = 13$) tissue microarrays were stained with either cytokeratin or S100, respectively, to create a tumor mask. PBR-TSPO immunofluorescence staining intensity was quantitated in tumor cells by AQUA. Representative sections demonstrating tissue with higher and lower PBR-TSPO expression is shown for NSCLC and melanoma cases.

[^{11}C]PBR28, arterial sampling is required, which further limits its clinical application. For [^{11}C]MET, SUV or SUVR images can be used in lieu of arterial sampling. In our study, [^{11}C]MET identified TR in all cases with an uptake rate constant K_i >2.00. If using the [^{11}C]MET SUV cutoff of >1.3 as recommended by the Joint EANM/EANO/RANO guidelines, then one of the lesions in our series would become a false positive (Supplemental Table S1).[13] [^{11}C]PBR28 did not reliably identify RN and did not add information in combination with [^{11}C]MET PET to confirm TR. Based on our small sample size, we cannot determine the extent to which concurrent corticosteroid or checkpoint inhibitor use affected PBR-TSPO expression, as 50% of those on corticosteroids still had [^{11}C]PBR28 avidity in RN lesions. Additionally, patients 1 and 3 had received PD-1 inhibitors around the time of SRS but half lacked [^{11}C]PBR28 avidity in the RN lesion. Although lung cancers have decreased

PBR-TSPO expression compared to normal lung,[32] we found protein levels were still significantly elevated to compromise the utility of [^{11}C]PBR28 to distinguish tumor cells from RN. We confirmed that multiple NSCLC and melanoma cell lines and tumor tissue revealed tumor expression of PBR-TSPO. Even though tumor cells had significantly less PBR-TSPO expression compared to monocytes, this level of expression compared to normal brain was sufficient to be a confounder leading to poor accuracy of [^{11}C]PBR28 in detecting RN. Since the initial design of this study, additional data regarding PBR-TSPO's role in promoting cancer cell survival has emerged.[32] While the mean time between lesion radiation and study imaging was 13.6 months (range 8.3-21.3 months), little is known how PBR-TSPO expression levels fluctuate post radiation. Further animal models may help elucidate the temporal expression changes post radiation.

A better understanding of the cellular and molecular processes underlying the development of RN is necessary to prevent and minimize radiation-associated morbidity and to improve treatment strategies, particularly as an increasing number of patients are receiving immunotherapy with SRS. The pathobiology of RN remains to be elucidated, but theories center on ischemia resulting from either radiation damage to the blood endothelial cells, due to demyelination by damaged glial cells, or as a result of an exuberant host immunologic response, which could be amplified by immunotherapy. Identifying critical mediators in RN, particularly in the setting of use of systemic immunotherapy, might facilitate development of tracers specific for RN. Additional imaging targets with potential clinical translation include poly(ADP-ribose) polymerase inhibitor [^{18}F]PARPi,[33] ^{18}F-fluoromisonidazole, 4-borono-2-[^{18}F]-fluoro-phenylalanine, [^{18}F]-fluoromethyl-dimethyl-2-hydroxyethylammonium (^{18}F-fluoromethylcholine), 3′-deoxy-3′-^{18}F-fluorothymidine (FLT),[7] 2-deoxy-2-(18)F-fluoro-d-mannose,[34] iodine-131-iododeoxyuridine,[35] and ^{124}I-labeled gold nanostar probes.[36] Furthermore, additional imaging modalities are actively being investigated, including SPECT and perfusion MRI.[37]

Conclusions

We demonstrate that the use of dual tracers is feasible and well-tolerated. Other RN-specific tracers are needed, as [^{11}C]PBR28 PET failed to reliably discriminate between TR and RN. Use of [^{11}C]MET as a single TR-specific tracer is promising but has limited implementation into standard practice due to tracer stability. Additional tracers are critically needed, particularly as the incidence of RN increases with combined immune therapy and SRS use.

Authors' Note

Trial Information: ClinicalTrials.gov NCT02433171 (https://clinicaltrials.gov/ct2/show/NCT02433171). Thuy T. Tran and Jean-Dominique Gallezot contributed equally. Veronica L. Chiang and Richard Carson contributed equally.Since the study was conducted, Dr. Gabriela Turcu is now affiliated with the Department of Dermatology, Colentina Clinical Hospital, Faculty of Medicine, Carol Davila University of Medicine and Pharmacy, Bucharest, Romania.

Declaration of Conflicting Interests

The author(s) declared the following potential conflicts of interest with respect to the research, authorship, and/or publication of this article. Dr. Harriet Kluger reports research grants from Merck, Bristol-Myers Squibb, and Apexigen during the conduct of the study, and personal fees from Merck, Regeneron, Alexion, Prometheus, Corvus, Nektar, Biodesix, Roche-Genetech, Pfizer, Iovance, Immunocore, Array Biopharma, and Celldex, outside of the submitted work. Dr. Chiang reports personal fees from Brainlab, Monteris Medical, and MRI Interventions outside of the submitted work. The other authors declare no conflicts of interest.

Funding

The author(s) disclosed receipt of the following financial support for the research, authorship, and/or publication of this article: This study was funded in part by the NIH [grant numbers R01 CA158167; K24CA172123; R01 CA227473; P50 CA121974; R01 CA204002; 1T32 CA233414; K12 CA2151103]; a grant from the Lung Cancer Research Foundation-LUNGevity and Melanoma Research Alliance [grant number 308721]; and a pilot grant from the Yale School of Medicine supporting new cancer studies for PET.

ORCID iD

Thuy T. Tran, MD, PhD https://orcid.org/0000-0002-6244-7575

Supplemental Material

Supplemental material for this article is available online.

References

1. Miyatake S, Nonoguchi N, Furuse M, et al. Pathophysiology, diagnosis, and treatment of radiation necrosis in the brain. *Neurol Med Chir (Tokyo)*. 2015;55(1):50–59. doi:10.2176/nmc.ra.2014-0188
2. Vellayappan B, Tan CL, Yong C, et al. Diagnosis and management of radiation necrosis in patients with brain metastases. *Front Oncol*. 2018;8:395. doi:10.3389/fonc.2018.00395
3. Gotz I, Grosu AL. [(18)F]FET-PET imaging for treatment and response monitoring of radiation therapy in malignant glioma patients—a review. *Front Oncol*. 2013;3:104. doi:10.3389/fonc.2013.00104
4. Sogani SK, Jena A, Taneja S, et al. Potential for differentiation of glioma recurrence from radionecrosis using integrated (18)F-fluoroethyl-L-tyrosine (FET) positron emission tomography/magnetic resonance imaging: a prospective evaluation. *Neurol India*. 2017;65(2):293–301. doi:10.4103/neuroindia.NI_101_16
5. Piroth MD, Liebenstund S, Galldiks N, et al. Monitoring of radiochemotherapy in patients with glioblastoma using O-(2-(1)(8)Fluoroethyl)-L-tyrosine positron emission tomography: is dynamic imaging helpful? *Mol Imaging*. 2013;12(6):388–395.
6. Lohmann P, Kocher M, Ceccon G, et al. Combined FET PET/MRI radiomics differentiates radiation injury from recurrent brain metastasis. *Neuroimage Clin*. 2018;20:537–542. doi:10.1016/j.nicl.2018.08.024

7. Zikou A, Sioka C, Alexiou GA, et al. Radiation necrosis, pseudoprogression, pseudoresponse, and tumor recurrence: imaging challenges for the evaluation of treated gliomas. *Contrast Media Mol Imaging*. 2018;2018:6828396. /01/11. doi:10.1155/2018/6828396
8. Glaudemans AW, Enting RH, Heesters MA, et al. Value of 11C-methionine PET in imaging brain tumours and metastases. *Eur J Nucl Med Mol Imaging*. 2013;40(4):615–635. doi:10.1007/s00259-012-2295-5
9. Yomo S, Oguchi K. Prospective study of (11)C-methionine PET for distinguishing between recurrent brain metastases and radiation necrosis: limitations of diagnostic accuracy and long-term results of salvage treatment. *BMC Cancer*. 2017;17(1):713. doi:10.1186/s12885-017-3702-x
10. Garcia JR, Cozar M, Baquero M, et al. The value of (11)C-methionine PET in the early differentiation between tumour recurrence and radionecrosis in patients treated for a high-grade glioma and indeterminate MRI. *Rev Esp Med Nucl Imagen Mol*. 2017;36(2):85–90. doi:10.1016/j.remn.2016.06.002
11. Deng SM, Zhang B, Wu YW, et al. Detection of glioma recurrence by (1)(1)C-methionine positron emission tomography and dynamic susceptibility contrast-enhanced magnetic resonance imaging: a meta-analysis. *Nucl Med Commun*. 2013;34(8):758–766. doi:10.1097/MNM.0b013e328361f598
12. Nihashi T, Dahabreh IJ, Terasawa T. Diagnostic accuracy of PET for recurrent glioma diagnosis: a meta-analysis. *AJNR Am J Neuroradiol*. 2013;34(5):944–950, S941-911. doi:10.3174/ajnr.A3324
13. Law I, Albert NL, Arbizu J, et al. Joint EANM/EANO/RANO practice guidelines/SNMMI procedure standards for imaging of gliomas using PET with radiolabelled amino acids and [(18)F]FDG: version 1.0. *Eur J Nucl Med Mol Imaging*. 2019;46(3):540–557. doi:10.1007/s00259-018-4207-9
14. Werry EL, Bright FM, Piguet O, et al. Recent developments in TSPO PET imaging as a biomarker of neuroinflammation in neurodegenerative disorders. *Int J Mol Sci*. 2019;20(13):3161. doi:10.3390/ijms20133161
15. Ruksha T, Aksenenko M, Papadopoulos V. Role of translocator protein in melanoma growth and progression. *Arch Dermatol Res*. 2012;304(10):839–845. doi:10.1007/s00403-012-1294-5
16. Han Z, Slack RS, Li W, Papadopoulos V. Expression of peripheral benzodiazepine receptor (PBR) in human tumors: relationship to breast, colorectal, and prostate tumor progression. *J Recept Signal Transduct Res*. 2003;23(2-3):225–238. doi:10.1081/RRS-120025210
17. Lumniczky K, Szatmari T, Safrany G. Ionizing radiation-induced immune and inflammatory reactions in the brain. *Front Immunol*. 2017;8:517. doi:10.3389/fimmu.2017.00517
18. Cuccurullo V, Di Stasio GD, Cascini GL, et al. The molecular effects of ionizing radiations on brain cells: radiation necrosis vs. tumor recurrence. *Diagnostics (Basel)*. 2019;9(4):127. doi:10.3390/diagnostics9040127
19. Chen MK, Guilarte TR. Translocator protein 18 kDa (TSPO): molecular sensor of brain injury and repair. *Pharmacol Ther*. 2008;118(1):1–17. doi:10.1016/j.pharmthera.2007.12.004
20. Alomari A, Rauch PJ, Orsaria M, et al. Radiologic and histologic consequences of radiosurgery for brain tumors. *J Neurooncol*. 2014;117(1):33–42. doi:10.1007/s11060-014-1359-8
21. Kreisl WC, Fujita M, Fujimura Y, et al. Comparison of [(11)C]-(R)-PK 11195 and [(11)C]PBR28, two radioligands for translocator protein (18 kDa) in human and monkey: implications for positron emission tomographic imaging of this inflammation biomarker. *NeuroImage*. 2010;49(4):2924–2932. doi:10.1016/j.neuroimage.2009.11.056
22. Deloar HM, Fujiwara T, Nakamura T, et al. Estimation of internal absorbed dose of L-[methyl-11C]methionine using whole-body positron emission tomography. *Eur J Nucl Med*. 1998;25(6):629–633.
23. Brown AK, Fujita M, Fujimura Y, et al. Radiation dosimetry and biodistribution in monkey and man of 11C-PBR28: a PET radioligand to image inflammation. *J Nucl Med*. 2007;48(12):2072–2079. doi:10.2967/jnumed.107.044842
24. Jin X, Mulnix T, Gallezot JD, Carson RE. Evaluation of motion correction methods in human brain PET imaging—a simulation study based on human motion data. *Med Phys*. 2013;40(10):102503. doi:10.1118/1.4819820
25. Carson RE, Barker W, Liow J-S, et al. Design of a motion-compensation OSEM list-mode algorithm for resolution-recovery reconstruction of the HRRT. *IEEE Nucl Sci Symp Conf Rec*. 2003; M16–6.
26. Patlak CS, Blasberg RG. Graphical evaluation of blood-to-brain transfer constants from multiple-time uptake data. Generalizations. *J Cereb Blood Flow Metab*. 1985;5(4):584–590. doi:10.1038/jcbfm.1985.87
27. Patlak CS, Blasberg RG, Fenstermacher JD. Graphical evaluation of blood-to-brain transfer constants from multiple-time uptake data. *J Cereb Blood Flow Metab*. 1983;3(1):1–7. doi: 10.1038/jcbfm.1983.1
28. Ichise M, Toyama H, Innis RB, Carson RE. Strategies to improve neuroreceptor parameter estimation by linear regression analysis. *J Cereb Blood Flow Metab*. 2002;22(10):1271–1281. doi:10.1097/00004647-200210000-00015
29. Ichise M, Liow J-S, Lu J-Q, et al. Linearized reference tissue parametric imaging methods: application to [11C]DASB positron emission tomography studies of the serotonin transporter in human brain. *J Cereb Blood Flow Metab*. 2003;23(9):1096–1112. doi:10.1097/01.WCB.0000085441.37552.CA
30. Camp RL, Chung GG, Rimm DL. Automated subcellular localization and quantification of protein expression in tissue microarrays. *Nat Med*. 2002;8(11):1323–1327. doi:10.1038/nm791
31. Owen DR, Yeo AJ, Gunn RN, et al. An 18-kDa translocator protein (TSPO) polymorphism explains differences in binding affinity of the PET radioligand PBR28. *J Cereb Blood Flow Metab*. 2012;32(1):1–5. doi:10.1038/jcbfm.2011.147
32. Bhoola NH, Mbita Z, Hull R, Dlamini Z. Translocator protein (TSPO) as a potential biomarker in human cancers. *Int J Mol Sci*. 2018;19(8):2176. doi:10.3390/ijms19082176
33. Donabedian PL, Kossatz S, Engelbach JA, et al. Discriminating radiation injury from recurrent tumor with [(18)F]PARPi and amino acid PET in mouse models. *EJNMMI Res*. 2018;8(1):59. doi:10.1186/s13550-018-0399-z

34. Furumoto S, Shinbo R, Iwata R, et al. In vitro and in vivo characterization of 2-deoxy-2-18F-fluoro-D-mannose as a tumor-imaging agent for PET. *J Nucl Med*. 2013;54(8):1354–1361. doi:10.2967/jnumed.112.113571
35. Tjuvajev JG, Macapinlac HA, Daghighian F, et al. Imaging of brain tumor proliferative activity with iodine-131-iododeoxyuridine. *J Nucl Med*. 1994;35(9):1407–1417.
36. Liu Y, Carpenter AB, Pirozzi CJ, et al. Non-invasive sensitive brain tumor detection using dual-modality bioimaging nanoprobe. *Nanotechnology*. 2019;30(27):275101. doi:10.1088/1361-6528/ab0e9c
37. Weber W, Bartenstein P, Gross MW, et al. Fluorine-18-FDG PET and iodine-123-IMT SPECT in the evaluation of brain tumors. *J Nucl Med*. 1997;38(5):802–808.